

# Evolution of galactic planes of satellites in the EAGLE simulation

Shi Shao,<sup>1\*</sup> Marius Cautun<sup>1</sup> and Carlos S. Frenk<sup>1</sup>

<sup>1</sup>*Institute for Computational Cosmology, Department of Physics, Durham University, South Road Durham DH1 3LE, UK*

8 July 2019

## ABSTRACT

We study the formation of planes of dwarf galaxies around Milky Way (MW)-mass haloes in the EAGLE galaxy formation simulation. We focus on satellite systems similar to the one in the MW: spatially thin or with a large fraction of members orbiting in the same plane. To characterise the latter, we introduce a robust method to identify the subsets of satellites that have the most co-planar orbits. Out of the 11 MW classical dwarf satellites, 8 have highly clustered orbital planes whose poles are contained within a  $22^\circ$  opening angle centred around  $(l, b) = (182^\circ, -2^\circ)$ . This configuration stands out when compared to both isotropic and typical  $\Lambda$ CDM satellite distributions. Purely flattened satellite systems are short-lived chance associations and persist for less than 1 Gyr. In contrast, satellite subsets that share roughly the same orbital plane are longer lived, with half of the MW-like systems being at least 4 Gyrs old. On average, satellite systems were flatter in the past, with a minimum in their minor-to-major axes ratio about 9 Gyrs ago, which is the typical infall time of the classical satellites. MW-like satellite distributions have on average always been flatter than the overall population of satellites in MW-mass haloes and, in particular, they correspond to systems with a high degree of anisotropic accretion of satellites. We also show that torques induced by the aspherical mass distribution of the host halo channel some satellite orbits into the host’s equatorial plane, enhancing the fraction of satellites with co-planar orbits. In fact, the orbital poles of co-planar satellites are tightly aligned with the minor axis of the host halo.

**Key words:** methods: numerical – galaxies: haloes – galaxies: kinematics and dynamics

## 1 INTRODUCTION

The Milky Way (MW) satellites have a highly inhomogeneous and anisotropic phase-space distribution whose origin remains one of the most baffling cosmological mysteries. All the classical dwarfs and many of the ultra-faint ones lie on a plane which shows an unexpectedly high degree of flattening (e.g. Kunkel & Demers 1976; Lynden-Bell 1976, 1982; Kroupa et al. 2005; Pawlowski 2016). Many of the satellites have orbits within this plane (e.g. Metz et al. 2008; Pawlowski & Kroupa 2013; Fritz et al. 2018) and the classical dwarfs have orbits that are more circularly biased than predicted by the current cosmological model (Cautun & Frenk 2017). Furthermore, the plane in which most of the satellites reside is nearly perpendicular to the MW disc (e.g. Lynden-Bell 1982; Libeskind et al. 2007; Deason et al. 2011; Shao et al. 2016), in contrast with observations of external galaxies where most satellites are found within the disc plane of the central galaxy (e.g. Brainerd 2005; Yang et al. 2006; Agustsson & Brainerd 2010; Nierenberg et al. 2012).

Observational studies have reveal that flattened satellite distributions similar to the MW system are ubiquitous. Our two nearest giant neighbours, M31 and Centaurus A, both have one or more planes of satellite galaxies (e.g. Conn et al. 2013; Shaya & Tully

2013; Tully et al. 2015), with many of their members showing correlated line-of-sight velocities that potentially indicate co-rotating configuration (Ibata et al. 2013; Müller et al. 2018; Hodkinson & Scholtz 2019). Farther afield, Cautun et al. (2015a) have shown that external galaxies also have anisotropic satellite distributions.

Within the standard cosmological model, the anisotropic distribution of satellites is a manifestation of the preferential direction of accretion into haloes (e.g. Aubert et al. 2004; Knebe et al. 2004; Zentner et al. 2005; Deason et al. 2011; Wang et al. 2014; Shi et al. 2015; Buck et al. 2015). The plane of satellites most likely reflects the connection between a galaxy and its cosmic web. Multiple satellites are accreted along the same filament (Libeskind et al. 2005; Buck et al. 2015) which leads to a significant population of co-rotating satellites (Libeskind et al. 2009; Lovell et al. 2011; Cautun et al. 2015a). Correlated satellite orbits can arise from the accretion of dwarf galaxy groups (e.g. Li & Helmi 2008; Wang et al. 2013; Smith et al. 2016; Shao et al. 2018a). However, the MW plane of satellites is unlikely to have originated from the accretion of most of the satellites either in one group or along one filament (Shao et al. 2018a, see also Metz et al. 2009; Pawlowski et al. 2012).

Most studies of the MW plane of satellites have focused on the population of classical satellites because these objects are the ones with the most precise proper motion measurements (e.g. Gaia Collaboration et al. 2018) and because we have only a partial census

\* E-mail: shi.shao@durham.ac.uk

of fainter satellites, with more than half of the predicted population of MW ultra-faint dwarfs awaiting discovery (Newton et al. 2018). While most  $\Lambda$ CDM haloes have planes of satellite galaxies, the properties of each plane vary from system to system (Cautun et al. 2015b) indicating that the planes encode information about the formation history of the host. For example, Shao et al. (2016) showed that while most dark matter haloes are aligned with their central galaxies, this might not be the case for the MW, and is a consequence of the Galactic plane of satellites being nearly perpendicular on the MW disc. A plane of satellites could also indicate a major merger during the evolution of the host (e.g. Hammer et al. 2013; Smith et al. 2016; Banik et al. 2018).

Most  $\Lambda$ CDM planes of satellite galaxies are transient features, with their thickness and orientation varying in time (Bahl & Baumgardt 2014; Buck et al. 2016). This is a result of many of the members not moving within the plane and also due to gravitational interactions between satellites, which have the net effect of diminishing phase space correlations (e.g. Fernando et al. 2017, 2018). The same holds true for the Galactic plane of satellites, since several of the classical dwarfs orbit outside the plane (e.g. Gaia Collaboration et al. 2018). Moreover the MW has the Large Magellanic Cloud (LMC) which is thought to be massive (Peñarrubia et al. 2016; Shao et al. 2018b; Cautun et al. 2019) and thus might also perturb the orbits of the other satellites (e.g. Gómez et al. 2015). Even in the ideal case, that is when assuming a spherical MW halo and when neglecting satellite interactions, the Galactic plane of satellites is short lived and loses its thinness in  $\sim 1$  Gyr (Lipnicky & Chakrabarti 2017, the proper motion errors make the timescale somewhat uncertain – e.g. see Pawlowski et al. 2017).

In this paper we study the formation and evolution of planes of satellite galaxies similar to the one observed in our galaxy. For this, we use the EAGLE galaxy formation simulation (Schaye et al. 2015) which is ideal for this study since it contains a large sample of MW-mass haloes with satellite populations similar to the MW classical dwarfs. We start by identifying analogues of the MW system in terms of either the thinness or the degree of coherent rotation of the satellite distribution. We study the stability of the planes of satellites and how the phase-space distribution of satellites in these systems compares with that of the overall population of MW-mass haloes. In particular, we focus the analysis on systems where most satellites orbit roughly in the same plane, since these are both the most stable planes and also the ones that contain the largest amount of information about the accretion history of the MW satellites.

The paper is organised as follows. Section 2 reviews the EAGLE simulation and describes our sample selection; Section 3 introduces the two methods we use for identifying planes of satellite galaxies; Section 4 presents our results on the formation and evolution of planes of satellites; we conclude with a short summary in Section 5.

## 2 OBSERVATIONAL AND SIMULATION DATA

Here we give an overview of the MW data and the galaxy formation simulation used in our study. We also describe the selection criteria of our sample of MW-like systems and how we follow the evolution of these systems across multiple simulation outputs.

### 2.1 Observational data

We study the spatial and orbital distribution of the 11 classical dwarfs of our galaxy. This choice is motivated by two consid-

erations. Firstly, it is thought that the classical dwarfs are bright enough that we have a nearly complete census of them. Secondly, we need galaxy formation simulations that contain a large number of MW-mass haloes. Such simulations have limited resolution, and even state-of-the-art ones, such as EAGLE, resolve only the most massive substructures of MW-mass haloes.

We use the sky coordinates, distances and radial velocities of the classical dwarfs from the McConnachie (2012) compilation. The satellite proper motion are taken from the Gaia DR2 release (Gaia Collaboration et al. 2018), except for the Leo I and II satellites, for which we use the HST proper motions since they have lower uncertainties (Sohn et al. 2013; Piatek et al. 2016). We then transform the satellite coordinates and velocities to the Galactic Centre reference frame (for details see Cautun et al. 2015b). The thickness of the satellite plane (see Eq. 1) and the orbital pole directions are calculated in this Galactic Centre frame.

### 2.2 The EAGLE simulation

We make use of the main cosmological hydrodynamical simulation (labelled Ref-L0100N1504) performed as part of the EAGLE project (Schaye et al. 2015; Crain et al. 2015). The main EAGLE run is ideal for this work since: i) due to its large volume, it contains a large number of MW-mass haloes, ii) it has a high enough resolution to resolve satellites similar to the classical dwarfs and follow their orbits, and iii) resolves the baryonic processes that affect the orbits of satellites, such as torquing and tidal stripping due to the presence of a central galaxy disc (see e.g. Ahmed et al. 2017).

The main EAGLE run simulates a periodic cube of 100 Mpc side length using  $1504^3$  dark matter particles and an equal number of baryonic particles. The dark matter particles have a mass of  $9.7 \times 10^6 M_{\odot}$ , while the gas particles have an initial mass of  $1.8 \times 10^6 M_{\odot}$ . EAGLE assumes a *Planck* cosmology (Planck Collaboration XVI 2014) and uses galaxy formation models calibrated to reproduce: the stellar mass function, the distribution of galaxy sizes, and the relation between supermassive black hole mass and host galaxy mass.

We make use of the EAGLE halo and galaxy merger trees described in McAlpine et al. (2016). Haloes and galaxies were identified using the SUBFIND code (Springel et al. 2001; Dolag et al. 2009) applied to the full matter distribution (dark matter, gas and stars). It consist of first identifying friends-of-friends (FOF) haloes using a linking length of 0.2 times the mean particle separation (Davis et al. 1985), after which each FOF halo is split into gravitationally bound substructures. The most massive subhalo is classified as the main halo and its stellar distribution as the central galaxy. The main haloes are characterized by the mass,  $M_{200}$ , and radius,  $R_{200}$ , that define an enclosed spherical overdensity of 200 times the critical density. The position of each subhalo and galaxy is given by the particle that has the lowest gravitational potential energy. The merger tree was built on top of the SUBFIND catalogues using the D-TREES algorithm (Jiang et al. 2014). The method works by tracing the most bound particles associated with each subhalo, and identifying in the subsequent simulation outputs the subhalo which contains the largest fraction of these particles.

### 2.3 Sample selection

To identify systems similar to the MW, we start by selecting the 3209 present day haloes with mass,  $M_{200} \in [0.3, 3] \times 10^{12} M_{\odot}$ . The wide mass range is motivated by the large uncertainties in

the mass of the MW (e.g. see Fig. 7 of Callingham et al. 2019) and the need to have a large sample of such systems. We require that any such halo be isolated and thus we remove any galaxy that has a neighbour within 600 kpc that has a stellar mass larger than half their mass. We also restrict our selection to systems that, like the MW, have at least 11 luminous satellites within a distance of 300 kpc from the central galaxy. We define luminous satellites as any subhaloes that has at least one stellar particle associated to them; this corresponds to objects with stellar mass higher than  $\sim 1 \times 10^6 M_\odot$ . We find 1080 host haloes that satisfy all three selection criteria, with the resulting sample having a median halo mass,  $M_{200} \sim 1.2 \times 10^{12} M_\odot$  (the distribution of host halo masses is shown in Fig. A1 of Shao et al. 2016).

To study the evolution of satellite systems, we make use of the EAGLE snapshots, which are finely spaced (about every 70 Myrs) simulation outputs that allow us to trace the orbits of satellites with very good time resolution. For each satellite and its central galaxy, we trace their formation history using the most massive progenitor in the merger trees. Starting at high redshift, we follow forward the merger tree of each satellite in tandem with the merger tree of its present day central galaxy, until we find the first snapshot where the satellite and the central are part of the same FOF group; we then define the epoch of that snapshot as the infall time for the satellite. In a small number of cases satellite galaxies may drift in and out of the host FOF halo. Even in those cases, we define the accretion time as the first time the satellite enters the progenitor of the  $z = 0$  host halo.

### 3 METHODS

Here we describe the two approaches we use to identify analogues of the MW planes of satellite galaxies: i) using the spatial distribution of satellites, which leads to determining *MW-like-thin* planes, and ii) using the orbital pole distribution, which leads to determining *MW-like-orbit* planes.

#### 3.1 *MW-like-thin* planes of satellite galaxies

We wish to identify planes of satellite galaxies that have a similar spatial distribution to the Galactic classical dwarfs, which we refer to as *MW-like-thin* planes. To find Galactic analogues, we calculate the thickness of the satellite systems using the mass tensor,

$$I_{ij} \equiv \sum_{k=1}^N x_{k,i} x_{k,j}, \quad (1)$$

where the sum is over the  $N = 11$  most massive satellites by stellar mass (hereafter the “top 11”). The quantity  $x_{k,i}$  denotes the  $i$ -th component ( $i = 1, 2, 3$ ) of the position vector of satellite  $k$  with respect to the central galaxy. The shape and the orientation are determined by the eigenvalues,  $\lambda_i$  ( $\lambda_1 \geq \lambda_2 \geq \lambda_3$ ), and the eigenvectors,  $\hat{e}_i$ , of the mass tensor. The major, intermediate and minor axes of the corresponding ellipsoid are given by  $a = \sqrt{\lambda_1}$ ,  $b = \sqrt{\lambda_2}$ , and  $c = \sqrt{\lambda_3}$ , respectively. We refer to  $c/a$  as the thickness of the satellite system and to  $\hat{e}_3$ , which points along the minor axis, as the normal to the plane of satellites.

The distribution of plane thicknesses,  $c/a$ , for the top 11 satellites of MW-mass hosts is shown in Fig. 1. The satellite systems have a large spread in  $c/a$  values ranging from  $\sim 0.15$  to  $\sim 0.9$  and a most likely value of  $c/a \approx 0.45$ . For comparison, we also show the shape,  $c/a$ , of their haloes, which is calculated by applying Eq.

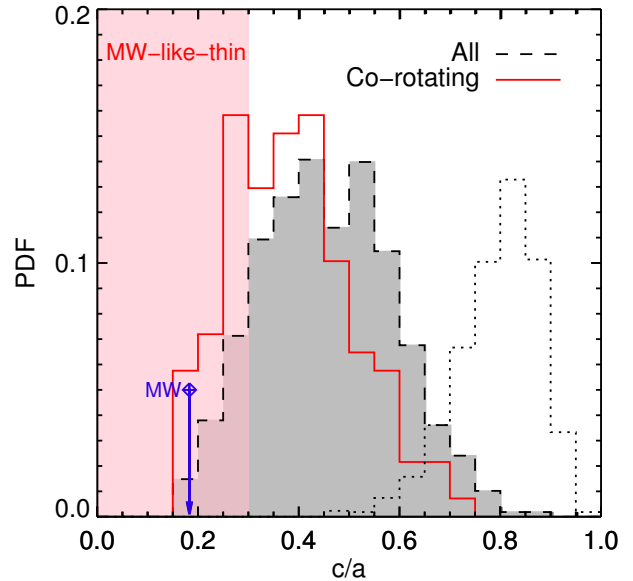


**Figure 1.** The axis ratio,  $c/a$ , distribution for the 11 most massive satellites of EAGLE MW-mass host haloes at  $z = 0$ . The dashed line corresponds to all haloes, while the solid line shows the hosts with an abundance of co-rotating satellites (see Sec. 3.2), that is hosts for which at least 8 of the 11 satellites have orbital planes within a  $35^\circ$  opening angle. The vertical arrow shows the Galactic value,  $c/a = 0.183$ . The red shaded region indicates systems with  $c/a < 0.3$ , which represent our EAGLE sample of *MW-like-thin* systems. The grey dotted line shows the  $c/a$  distribution of the mass for MW-mass dark matter haloes (to better fit the plot, the halo  $c/a$  PDF is normalized to 0.5 and not to unity).

(1) to the distribution of dark matter particles within  $R_{200}$  from the halo centre (see dotted line in Fig. 1). On average, the satellites are more flattened and have a wider distribution of  $c/a$  values than their host haloes (e.g. see also Libeskind et al. 2005; Kang et al. 2005).

The 11 classical dwarfs of the MW have an axis ratio,  $c/a = 0.183$ , which is shown by the vertical arrow in Fig. 1. This value is very low when compared with the typical expectation in EAGLE, with only  $\sim 1$  percent of EAGLE MW-mass haloes having thinner satellite distributions (see also Wang et al. 2013; Pawlowski et al. 2014). To obtain analogues to the MW planes of satellites, we select EAGLE systems with  $c/a < 0.3$ , which represents our sample of *MW-like-thin* planes. There are 134 such systems and they represent 12 percent of the total sample of EAGLE MW-mass haloes. Note that while most of the *MW-like-thin* planes are thicker than the MW one, the thickness of the MW plane of satellites is predicted to increase rapidly with time (e.g. see Lipnicky & Chakrabarti 2017) and thus our selection procedure is reasonable.

#### 3.2 *MW-like-orbit* planes of satellite galaxies

The MW classical satellites show a surprisingly high degree of coherent rotation, with many dwarfs orbiting in nearly the same plane (see Fig. 2). Here, we want to better characterise the orbital structure of the Galactic satellites and to identify similar satellite configurations in cosmological simulations. To do so, we start from the question: how many MW satellites orbit approximately in the same plane and which ones are those?

To answer the question, we first identify which subset of  $N$  out of 11 classical satellites has the most planar orbits, for  $N$  varying from 1 to 11. For each value of  $N$ , we calculate the direction which

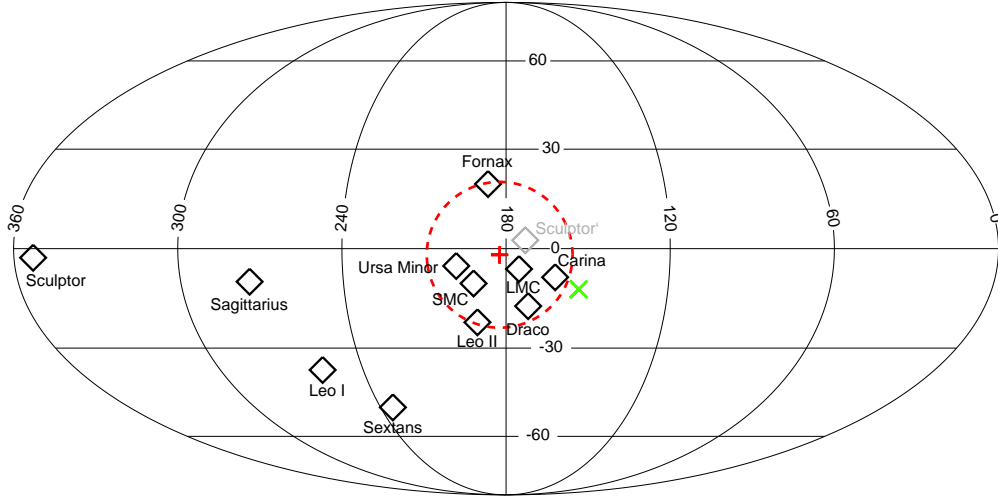


**Figure 2.** Aitoff projection of the orbital poles of the MW classical satellites. Each black rhombus corresponds to the orbital pole of a satellite in Galactic longitude,  $l$ , and latitude,  $b$ . Out of the 11 classical satellites, 8 orbit in roughly the same plane, that is within a  $22^\circ$  opening angle. The normal to this orbital plane is indicated by the red cross symbol and the dashed line shows a  $22^\circ$  opening angle around this direction. Out of the 8 satellites with co-planar orbits, Sculptor is counter-rotating and, to emphasize its membership in the orbital plane, the grey rhombus shows its position after flipping its orbital pole. The green x symbol shows the orientation of the minor axis of the spatial distribution of satellites.

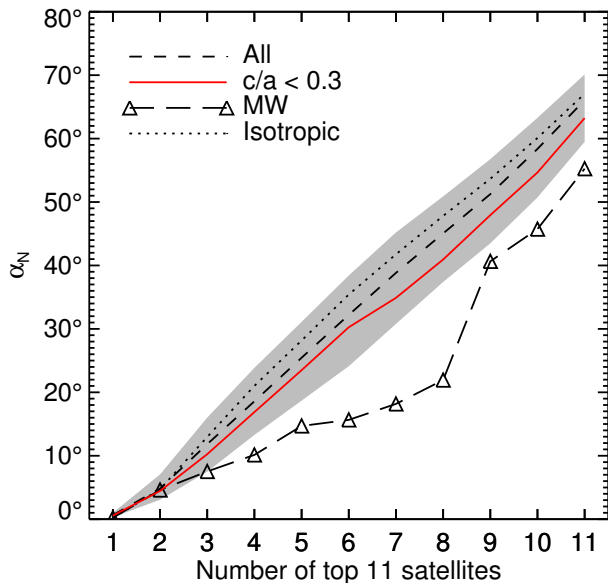


**Figure 3.** The distribution of opening angles,  $\alpha_N$ , corresponding to the  $N$  out of 11 satellites which have the most co-planar orbits. The dashed line shows the median value for all MW-mass systems in EAGLE and the grey shaded region shows the 16 to 84 percentiles. The dashed line with symbols shows the Galactic classical satellites, with the MW having 8 objects with very co-planar orbits. The solid line shows the median expectation for *MW-like-thin* systems, i.e. with  $c/a < 0.3$ . The dotted line shows the median expectation for isotropically distributed orbital planes.

contains within the smallest opening angle the orbital poles of  $N$  of the 11 satellites. We find this preferred direction by generating  $10^4$  uniformly distributed points on the unit sphere, which correspond to  $10^4$  uniformly distributed directions. For each direction,  $\hat{n}_i$ , we calculate its angle,

$$\Delta_{ij} = \arccos \left( |\hat{n}_i \cdot \hat{L}_j| \right), \quad (2)$$

with the direction of the orbital angular momentum,  $\hat{L}_j$ , of each of the 11 satellites. We take the absolute value of the  $\hat{n}_i \cdot \hat{L}_j$  scalar

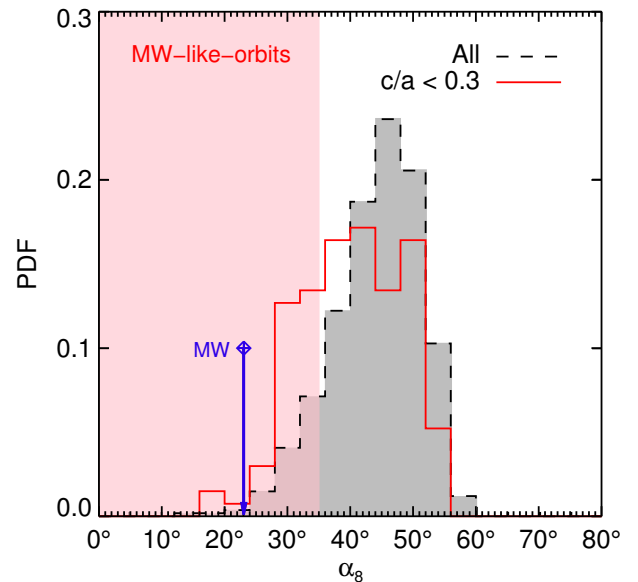


**Figure 4.** The distribution of opening angles,  $\alpha_8$ , corresponding to 8 out of the top 11 satellites with the most co-planar orbits. The dashed and solid lines correspond to all and  $c/a < 0.3$  MW-mass systems in EAGLE. The vertical line indicates the Galactic value,  $\alpha_8 = 22^\circ$ . The red shaded region corresponds to the selection of *MW-like-orbit* systems, that is those with  $\alpha_8 < 35^\circ$ .

product to account for the fact that satellites can be both co- and counter-rotating in the same plane. The  $N$  of the 11 satellites that come closest to rotating in the plane perpendicular to  $\hat{n}_i$  are the  $N$  galaxies with the smallest  $\Delta_{ij}$  angle. The largest of those  $N$  angles determines the minimum opening angle,  $\alpha_{N,i}$ , around the  $\hat{n}_i$  direction needed to enclose the orbital poles of all those  $N$  satellites. In practice, we implement this procedure by sorting the satellites in ascending order of their  $\Delta_{ij}$  angle, with the sequence of angles corresponding to the minimum opening angle,  $\alpha_{N,i}$  (with  $N$  from 1 to 11). We repeat this procedure for each of the  $10^4$  uniformly distributed directions to obtain a set of values  $\{\alpha_{N,i}\}$  with  $N = 1$  to 11 and  $i = 1$  to  $10^4$ .

**Table 1.** The distribution of the orbital poles of the classical satellites, given in terms of Galactic longitude,  $l$ , and latitude,  $b$ . The first 8 satellites in this table orbit in approximately the same plane whose normal is given by  $(l, b) = (182.3^\circ, -1.8^\circ)$  (see Fig. 2). The last column gives the angle,  $\Delta$ , between each orbital pole and the normal to this plane (see Eq. 2). The satellites are ordered in ascending order of the  $\Delta$  values.

Name	$l[^\circ]$	$b[^\circ]$	$\Delta[^\circ]$
<b>Satellites orbiting in nearly the same plane</b>			
LMC	175.3	-6.0	8.2
Sculptor <sup>†</sup>	353.0	-2.7	10.3
SMC	192.0	-10.3	12.9
Ursa Minor	198.3	-5.1	16.3
Draco	171.7	-17.1	18.5
Carina	161.9	-8.5	21.3
Fornax	186.8	19.3	21.6
Leo II	191.0	-22.0	21.9
<b>Satellites orbiting outside the plane</b>			
Sextans	234.1	-49.4	64.8
Leo I	257.0	-36.9	76.8
Sagittarius <sup>†</sup>	274.6	-9.8	88.0

<sup>†</sup>Sculptor and Sagittarius have counter-rotating orbits with respect to the plane normal. The other satellites have co-rotating orbits.

The subsample of  $N$  satellites which have the most co-planar orbits is obtained by finding the minimum over  $i$  of the  $\alpha_{N,i}$  values. We define the corresponding direction as the direction of the plane in which those  $N$  satellites rotate. The minimum opening angle,  $\alpha_N \equiv \min_i \alpha_{N,i}$ , describes how planar are the orbits of those satellites. The smaller  $\alpha_N$  is, the more clustered are the orbital poles of the  $N$  satellites.

To determine the optimal value of  $N$  for the MW, we study in Fig. 3 the dependence of the  $\alpha_N$  opening angle on  $N$ . This is shown in the figure by the dashed line with symbols. The  $\alpha_N$  variation with  $N$  for the MW system shows a curious trend: it increases slowly for small  $N$  and then exhibits a large rise as  $N$  is increased from 8 to 9. This is indicative of the MW having 8 classical satellites with roughly co-planar orbits, while the remaining 3 classical satellites orbit outside this plane. The same conclusion can be reached when comparing the Galactic orbits with the median expectation for an isotropic distribution of orbits (see dotted line in Fig. 3). For  $N \leq 8$ , the MW  $\alpha_N$  angle grows more slowly with  $N$  than the median expectation for isotropic orbits, while for  $N > 8$ , the slope of the two functions is roughly the same.

Fig. 3 also shows the distribution of  $\alpha_N$  values for the brightest 11 satellites of MW-mass haloes in EAGLE. This was obtained by applying to each EAGLE satellite system the same procedure as for the MW satellites. The figure shows the median value of  $\alpha_N$  (dashed line) and the 16 to 84 percentiles of the distribution (grey shaded region). The median  $\alpha_N$  angle of MW-mass hosts increases gradually with the number of satellites,  $N$ , and, at fixed  $N$ , its value is slightly lower than the median expectation for an isotropic distribution of orbits, which indicates that  $\Lambda$ CDM haloes have an excess of satellites that orbit roughly in the same plane. The MW  $\alpha_N$  values are systematically below the EAGLE results, and especially outside the 68 percentile region, indicating that the MW has a larger degree of co-planar satellite orbits than typically expected in  $\Lambda$ CDM. The difference in  $\alpha_N$  opening angles between the EAGLE sample and the MW is largest for  $N = 8$ , indicating again that the orbits of 8 of the classical satellites are much more co-planar than expected.

Fig. 2 presents the distribution of orbital poles for the 11 classical satellites of the MW. The 8 of them with the largest orbital coplanarity are the ones shown inside the red-dashed circle, which corresponds to an opening angle  $\alpha_8 = 21.9^\circ$ . This is the minimum opening angle need to enclose the orbital poles of those satellites. The centre of this circle is found at  $(l, b) = (182.3^\circ, -1.8^\circ)$  (see red cross symbol) and corresponds to the direction of the plane in which most of the MW satellites orbit currently. The angles between this plane and the orbital poles of each MW classical satellite are given in Table 1. Out of 8 satellites orbiting in the plane, 7 of them are co-rotating while one, i.e. Sculptor, is counter-rotating. To better emphasise that Sculptor orbits within the plane, the light grey symbol in Fig. 2 shows Sculptor's orbital pole if it were orbiting in the opposite direction. Using pre-Gaia data, the coherent alignment of 7 to 9 classical satellites has been pointed out by Pawlowski & Kroupa (2013). Note, however, that they employed a different method of identifying co-orbiting satellites that has one important difference compared with our approach: it does not allow for counter-rotating satellites.

Motivated by the analysis of the MW satellites shown in Figs. 2 and 3, we define *MW-like-orbit* planes as those for which at least 8 out of the 11 satellites orbit in a narrow plane (i.e. have a small  $\alpha_8$  value). We study such systems in Fig. 4, which shows the distribution of the opening angle,  $\alpha_8$ , for MW-mass haloes in EAGLE. The distribution is peaked at  $\alpha_8 = 45^\circ$ , and has a slowly decreasing tail for small  $\alpha_8$  values. When comparing to the MW  $\alpha_8$  value (which is show in Fig. 4 by a vertical arrow), we find that very few EAGLE systems have satellites with orbits as planar as in our own galaxy. In fact, less than 1 percent of EAGLE systems have  $\alpha_8 < 22^\circ$ , which is the Galactic value. To obtain a reasonable sample of rotating planes of satellites similar to the MW, we relax the  $\alpha_8$  threshold and define *MW-like-orbit* planes as those with  $\alpha_8 < 35^\circ$ ; this corresponds to roughly 13 percent of the EAGLE sample of MW-mass hosts.

### 3.3 Spatially thin and orbitally coherent planes of satellites

The classical satellites of our galaxy are found to have both a spatially thin configuration and also a majority of members rotating in nearly the same plane. This raises two intriguing questions: Do spatially thin satellite distributions have also a high degree of coherent orbits? and conversely, are satellite systems with many planar orbits also spatially thin?

We start by considering the first of the two questions. The solid red line in Fig. 4 shows the distribution of opening angles,  $\alpha_8$ , for the EAGLE *MW-like-thin* planes, that is those with  $c/a < 0.3$ . Compared to the full population, *MW-like-thin* satellite systems have systematically smaller  $\alpha_8$ ; however, the difference is small. Only 30 percent of the *MW-like-thin* planes are classified as having *MW-like-orbit* planes (i.e.  $\alpha_8 < 35^\circ$ ). This is only slightly larger than the 13 percent fraction of the overall population of MW-mass haloes that are classified as having *MW-like-orbit* planes. These results indicate that having thin planes of satellites does not imply also planar orbits. As we will see in the next section, most spatially thin planes are due to chance configurations and thus are short lived.

We now study the typical thickness of *MW-like-orbit* planes of satellites. The distribution of axes ratio,  $c/a$ , for systems with *MW-like-orbit* planes is shown by the solid red line in Fig. 1. Such system are typically thinner than the overall population, with the PDF shifted towards overall lower  $c/a$  values. About 30 percent of the *MW-like-orbit* planes are found to have  $c/a < 0.3$  and thus are classified as *MW-like-thin* planes. In general, *MW-like-orbit* planes

are not necessarily thin since to identify them we required that 8 out of the 11 satellites have nearly planar orbits. The other 3 satellites can have very different orbital planes and, at least for part of their orbit, can be found at large distances from the common orbital plane of the 8 satellites with the most planar orbits. Such configurations would result in a large minor axis,  $c$ , and thus large  $c/a$  ratios.

Many of the discussion points of this section apply to the Galactic plane of classical satellites. At the moment the plane is spatially thin; however, since at least 3 of the satellites are moving in a direction nearly perpendicular to the plane, it will stop being so in the near future (see e.g. the orbital modelling and analysis of Lipnicky & Chakrabarti 2017 and Gaia Collaboration et al. 2018). Thus, when identifying analogues to the Galactic plane of satellites, it does not make sense to be overly restrictive by selecting planes that are spatially thin and that also have a majority of members which orbit in the same plane. Such a selection would result in a small sample (40 out of the 1080 MW-mass haloes in EAGLE) without leading to much physical insight.

### 3.4 How common is the MW satellite system?

The flattening,  $c/a$ , and the  $\alpha_8$  opening angle of the MW classical satellites is atypical when compared to the EAGLE simulation. This can be easily seen from Figures 1 and 4 which show that our galaxy is in the tail of the distribution. Compared to the MW, out of our sample of 1080 satellite systems, 9 (0.8%) are thinner and 6 (0.6%) have smaller  $\alpha_8$  values. In particular, we find only one system that has lower  $c/a$  and  $\alpha_8$  values than our galaxy. This raises two crucial questions that we address in this subsection.

Firstly, does the rarity of the MW plane of satellites pose a challenge to the standard cosmological model? This question has been addressed by Cautun et al. (2015b) who showed that while many  $\Lambda$ CDM systems have planes of satellites, no two planes are the same: the number of satellites in the plane, the plane thickness and the number of members with coherent rotation vary from system to system. For example, there are many different ways of obtaining planar satellite orbits that are as infrequent as the MW case, such as having 9 out of 11 (instead of the MW's 8) satellites with orbital poles contained within a  $26^\circ$  (compared to the MW  $22^\circ$ ) opening angle – this is because the higher number of satellites compensates for the larger opening angle to result in a similarly uncommon configuration. This suggests that the MW plane of satellites is just one possible realisation out of a very diverse population of planes of satellites. Because of this very diversity, the frequency of a particular configuration of satellites, such as the MW one, cannot by itself be used to judge the success or failure of a given cosmological model.

Secondly, to obtain a reasonably large sample of *MW-like* systems our selection criteria are not excessively fine-tuned to match the exact MW satellite distribution. In particular, the *MW-like-thin* sample is defined adopting  $c/a < 0.3$  while the MW has  $c/a = 0.18$ , and the *MW-like-orbit* systems are defined adopting  $\alpha_8 < 35^\circ$  while for the MW  $\alpha_8 = 22^\circ$ . This raises the question: do our findings apply to the MW given that most of the systems we study are less extreme? We strongly suspect that is the case: the same processes that we see in the simulations for these less extreme systems are likely to have played at least some role in the formation of the Galactic plane of satellites. However, to answer this question unequivocally we would need to use hydrodynamic simulations of a much larger volume ( $\sim 100$  times larger than EAGLE to have useful samples) with at least the same resolution as EAGLE. We plan

to further study this topic once the ongoing EAGLE-XL simulation, whose goal is to have a 30 times higher volume than EAGLE, is completed.

## 4 RESULTS

In this section we study the time evolution of planes of satellite galaxies, beginning with a few individual examples and then focusing on the population of planar structures as a whole.

### 4.1 Evolution of individual planes

#### 4.1.1 MW-like-thin planes

We first study the time evolution of an EAGLE galactic mass halo that contains a *MW-like-thin* plane. We select a satellite system that at the present time is very flattened,  $c/a = 0.176$ . The flattening is roughly equal to that of our Galactic satellites, which have  $c/a = 0.183$ . The evolution of this system is shown in Fig. 5. The top panel shows the axes ratio,  $c/a$ , for the progenitors of the top 11 present-day satellites of this system. The thickness of the system varies rapidly with redshift: 2 Gyrs ago it was twice as thick,  $c/a > 0.4$ , while even further ago, it was as thin as at the present day.

The rapid time evolution of the  $c/a$  axes ratio is a consequence of the complex orbits of the system's members. Many members do not orbit within the  $z = 0$  plane of satellites and furthermore the orientation of their orbital angular momentum can vary in time. This is highlighted in the middle panel of Fig. 5, which shows the angle,  $\gamma$ , between the orbital angular momentum of each satellite and the  $z = 0$  minor axis,  $\hat{e}_{3,z=0}$ , of the satellite system. The evolution of each satellite is shown by a differently colour line. The line is shown as dotted before infall and becomes solid when the satellite falls into its host.

We find that some of the satellites have been orbiting in a plane aligned with the  $\hat{e}_{3,z=0}$  vector for at least several Gyrs. One such example is the top red line with star symbols which indicates a satellite whose orbital plane has been nearly constant: it has had a misalignment angle with  $\hat{e}_{3,z=0}$  smaller than  $30^\circ$  since at least 10 Gyrs ago, which is even before its infall into the host halo 7 Gyrs ago. However, a significant fraction of the satellites have an orbital angular momentum whose direction varies in time. One example is the satellite shown by the green line with rhombus symbols towards the bottom of the panel: at  $z = 0$  its angular momentum vector makes an angle  $\gamma \approx 180^\circ$  with  $\hat{e}_{3,z=0}$ , indicating that it is counter-rotating in the plane. This satellite was in a nearly perpendicular orbit 10 Gyrs ago and, since then, its orbit has been slowly becoming increasingly aligned with  $\hat{e}_{3,z=0}$ . An extreme example of an orbital plane change is shown by the cyan line with triangle symbols. The angular momentum of this satellite flipped nearly  $180^\circ$  between 5 and 3 Gyrs ago. The flip was due to a close approach and interaction with a massive satellite (the one in purple), which changed, at least temporarily, the orbit of the lower mass satellite.

The example system depicted in Fig. 5 illustrates that also the orientation of the plane of satellite orientation can vary with time. This is highlighted in the bottom panel of Fig. 5, which shows the misalignment angle between the normal,  $\hat{e}_3$ , to the satellite distribution at different epochs and its orientation,  $\hat{e}_{3,z=0}$ , at the present day<sup>1</sup>. While this misalignment angle has been roughly constant

<sup>1</sup> We take the absolute value of the dot product between the plane of satellite orientations at various times. This is because the planes are charac-

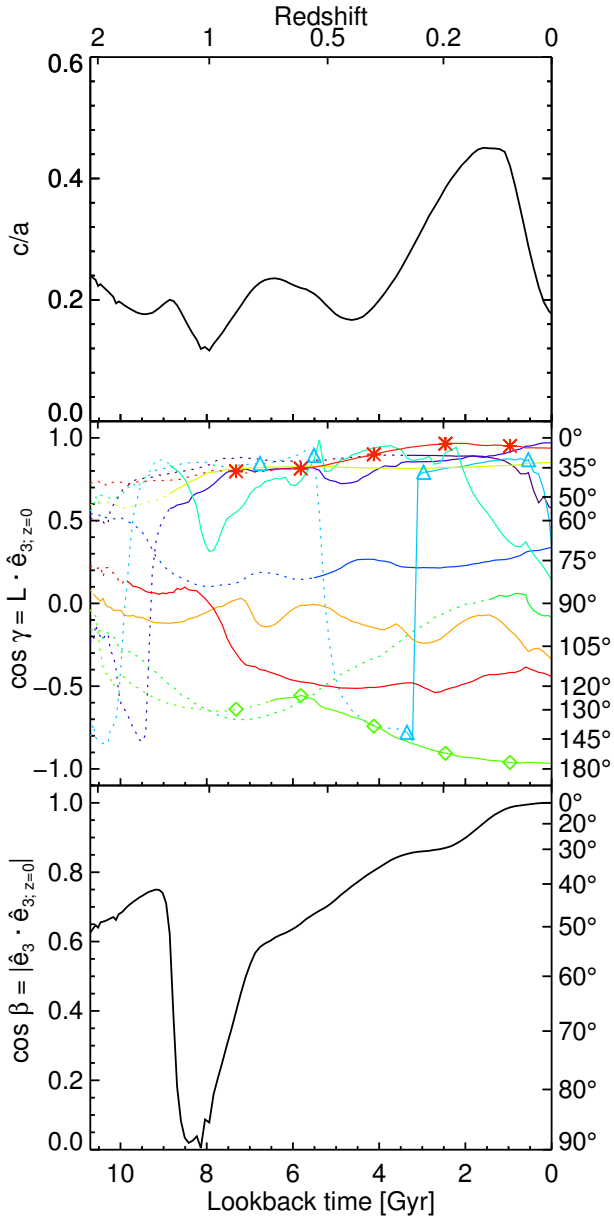


**Figure 5.** *Upper panel:* the evolution of  $c/a$  for the top 11 satellites of a *MW-like-thin* system from the EAGLE simulation. The satellite system has  $c/a = 0.176$  at  $z = 0$ , similar to the Galactic value of  $c/a = 0.182$ . *Middle panel:* the angle between the orientation,  $\hat{e}_{3,z=0}$ , of the  $z = 0$  plane of satellites and the angular momentum,  $L$ , of each satellite at different lookback times. Each colour line shows the main progenitor of each of the top 11 satellites. Each progenitor is shown as a dotted line before infall, and as a solid line after infall into the MW-mass host halo. The progenitors shown as lines with symbols are discussed in detail in the main text. *Bottom panel:* the evolution of the alignment angle between the orientation of the plane of satellites at  $z = 0$ ,  $\hat{e}_{3,z=0}$ , and the orientation at different lookback times,  $\hat{e}_3$ .

during the last 1 Gyr, before that it varied rapidly. In particular, 8 Gyrs ago the satellite distribution was even more planar than at the present day (with a minor to major axis ratio,  $c/a \sim 0.12$ ), however the orientation of that plane of satellites was perpendicu-

terised by an orientation and not a direction. Thus, the misalignment angle can be at most  $90^\circ$ .

lar to the  $z = 0$  plane of satellites. This indicates that *MW-like-thin* planes show a weak coherence between different times.

#### 4.1.2 *MW-like-orbit planes*

We now focus our attention on the evolution of satellite systems that have the same number of planar orbits as the MW. These are the *MW-like-orbit* planes (for details see Section 3.2). We illustrate the evolution of such planes of satellites by showing in Fig. 6 two examples from the EAGLE simulation that resemble closely the orbits of the classical MW satellites. The two examples have 8 out of its top 11 satellites orbiting within an opening angle,  $\alpha_8 = 22^\circ$  and  $24.5^\circ$ , respectively.

As was the case of *MW-like-thin* planes, the flattening of the two satellite systems varies rapidly with time (see the two top row panels in Fig. 6). While at least 8 of the satellites orbit within a plane, the other satellites can have very different orbital planes and the minor-to-major axis ratio,  $c/a$ , can vary as these satellites move in and out of the orbital plane shared by the 8 most co-planar satellites. In fact, the  $c/a$  ratio is so sensitive to individual satellites that even one single object orbiting in a perpendicular plane can lead to large values of  $c/a$ . This is the case for the example shown in the left column of Fig. 6, where 2 Gyrs ago the satellite distribution had a thickness,  $c/a \sim 0.52$ , that was predominantly due to one satellite moving in a direction perpendicular to the shared orbital plane (middle-row left-hand panel in Fig. 6).

If instead we consider the flattening of the 8 satellites with the most co-planar orbits, we find an axis ratio,  $c/a$ , that is considerably smaller and that varies considerably less with time. This is illustrated by the solid red line in the two top panels of Fig. 6. Nonetheless, even in this case the  $c/a$  ratio can vary with time since the satellite orbits are not perfectly planar and, as the satellites approach apocentre, they can find themselves at a larger height from the common orbital plane.

We now focus our analysis on the evolution of orbital planes of individual satellites, which are shown in the two middle panels of Fig. 6. The lines show the alignment angle between the orbital angular momentum,  $L$ , of a satellite at a given time and the  $z = 0$  direction,  $\mathbf{n}_{z=0}$ , of the common orbital plane of the 8 satellites with the most co-planar orbits. Alignment angles of  $\sim 0^\circ$  and  $\sim 180^\circ$  correspond to satellites that are co-rotating and counter-rotating with the common orbital plane, respectively. For the system shown in the left-hand column, most satellites are characterised by very early infall times,  $t < 9$  Gyrs, and have orbital poles that are roughly constant in time, especially within the last 4 Gyrs. By contrast, in the system shown in the right-hand column, the orbital poles of the satellites were very different at accretion and have converged slowly towards the present-day distribution when many of them share a common orbital plane. These two system illustrate the diversity of orbital histories that can lead to a majority of satellites with co-planar orbits.

Interestingly, the different orbital evolution of co-planar satellites translates into distinct predictions for the coherence of *MW-like-orbit* planes across cosmic times. This is highlighted in the bottom panels of Fig. 6 which show the alignment angle between the plane of satellites at earlier times and at  $z = 0$ . In particular, the system shown in the left-hand panel has a roughly constant orientation for the plane made of the 8 most co-planar satellites. In contrast, the system shown in the right-hand panel has a plane of satellites whose orientation has changed over time and only recently, within the last 6 Gyrs, has been roughly stable. This is a

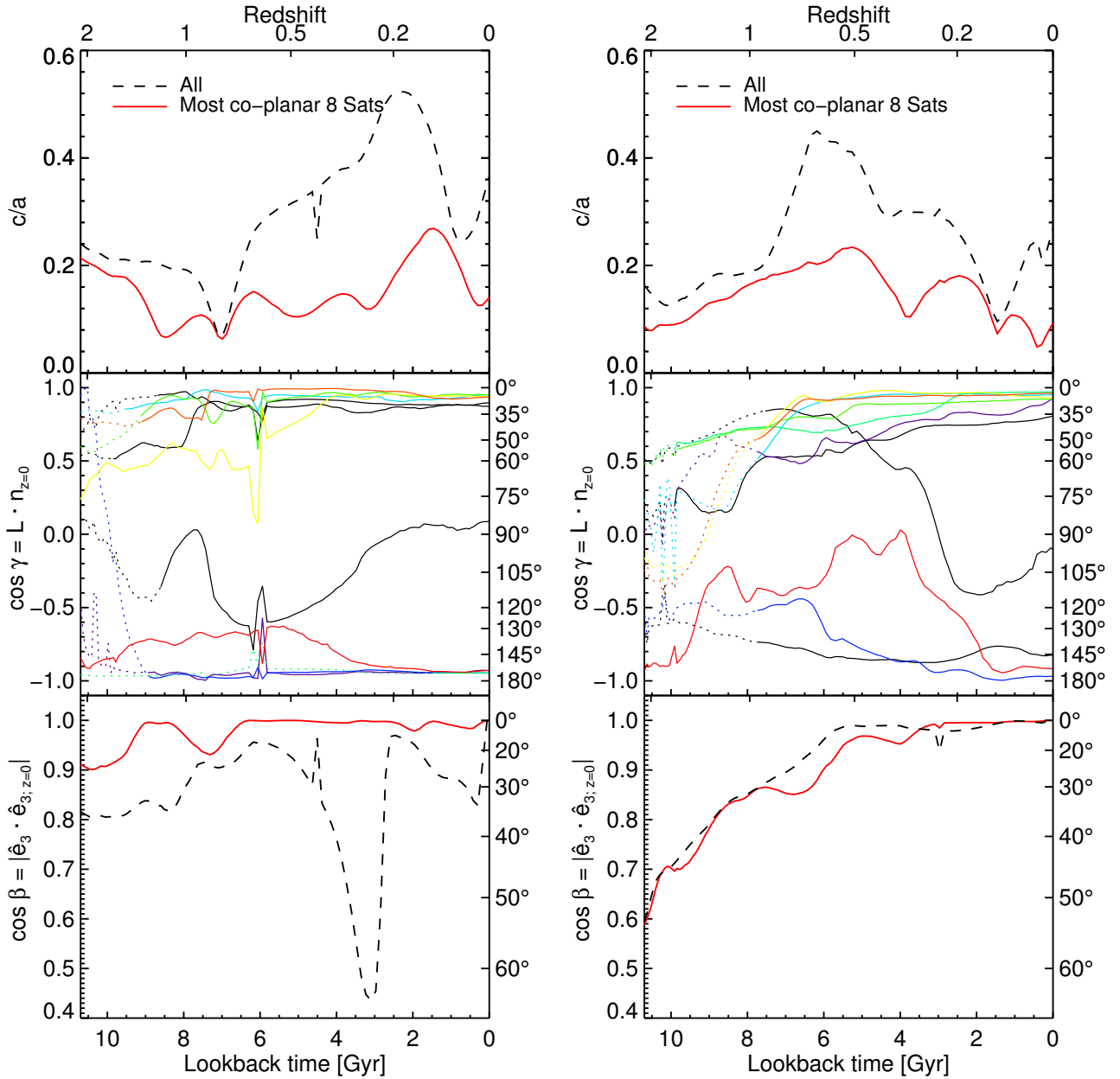


**Figure 6.** The evolution of two EAGLE MW-mass systems which have many co-planar satellite orbits at  $z = 0$ . The two columns correspond to systems with opening angle,  $\alpha_8 = 22^\circ$  (left column) and  $\alpha_8 = 24.5^\circ$  (right column). *Top panels:* the evolution of the axes ratio,  $c/a$ , for all 11 satellites (black dashed line) and for the 8 with the most co-planar orbits (red solid line). *Middle panels:* the alignment angle between the  $z = 0$  orientation,  $\mathbf{n}_{z=0}$ , of the orbital plane for the 8 most co-planar satellites and the angular momentum,  $\mathbf{L}$ , of the progenitors of the top 11 present-day satellites. The colour lines correspond to the 8 satellites with the most co-planar orbits. *Bottom panels:* the alignment angle between the orientation of the plane of satellites at  $z = 0$ ,  $\hat{\mathbf{e}}_{3,z=0}$ , and the orientation at different lookback times,  $\hat{\mathbf{e}}_3$ , for the top 11 satellites (black dashed line) and for the 8 satellites with the most co-planar orbits (red solid line).

manifestation of the present day co-planar satellites having very different orbital poles at high redshift.

## 4.2 Evolution of the shape and orientation of satellite systems

In this section we study the formation history of the plane of satellites population as a whole and assess to what extent the three satellite systems illustrated in the previous section are typical of the overall population of planes. As before, we focus the discussion on *MW-like-thin* and *MW-like-orbit* planes, which capture the two defining characteristics of the Galactic plane of satellites: its thinness and its high number of satellites with planar orbits.

### 4.2.1 The flattening of the overall population of satellite systems

We start by studying the time evolution of the spatial distribution of the top 11 brightest satellites. This is illustrated in the top row of Fig. 7, which shows the median values of the axes ratios,  $\langle c/a \rangle$  and  $\langle b/a \rangle$ , as a function of lookback time. The top-left-hand panel shows that the median  $c/a$  for the full sample of MW-mass systems decreases in the past, and indicates that satellite systems were typically thinner at higher redshift. The minimum of  $\langle c/a \rangle$  is found at a lookback time of  $\sim 9$  Gyrs (i.e. redshift  $z \sim 1.3$ ), when the satellite distribution was 60% flatter, that is a  $\langle c/a \rangle = 0.27$ , compared

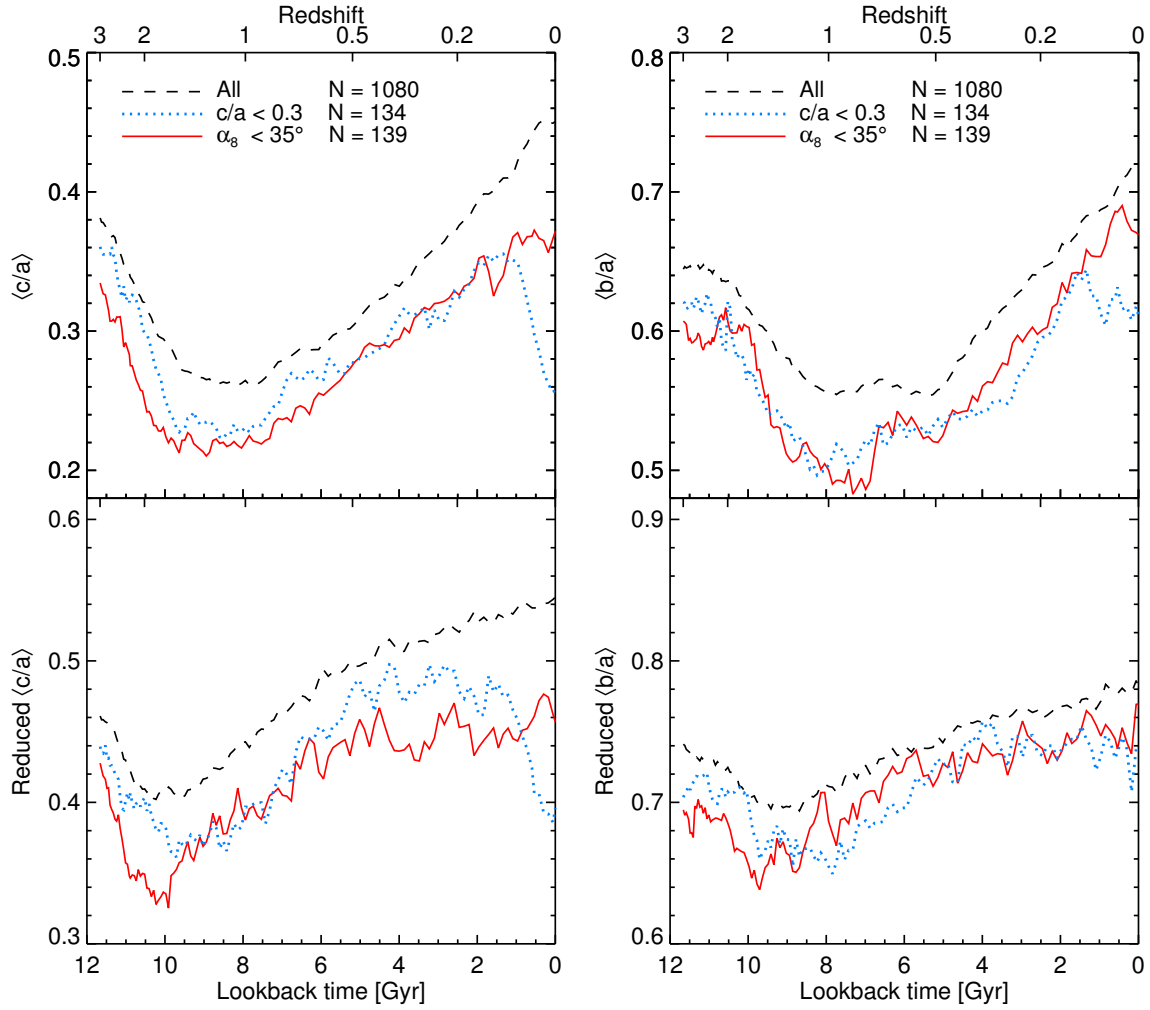


**Figure 7.** The time evolution of the median axes ratios,  $\langle c/a \rangle$  (left-hand column), and  $\langle b/a \rangle$  (right-hand column), for satellite systems of MW-mass haloes in the EAGLE simulation. We plot results for the entire population (dashed line) as well as for systems identified as having *MW-like-thin* (dotted line) and *MW-like-orbit* (solid line) planes. The bottom row shows  $\langle c/a \rangle$  and  $\langle b/a \rangle$  calculated using the reduced moment of inertia, that is by scaling each satellite coordinate by its distance from the host halo centre.

to the present-day value of 0.45. Further in the past, the flattening of the satellite distribution increases rapidly.

As we have seen in the previous section, the flattening of the satellite distribution can be affected by just a few satellites. For example, if the progenitor of one of the present-day satellites is far from the host (such as before accretion). This can result in a very large value for the major axis of the system without a corresponding increase in the value of the minor axis. This would give rise to a reduction of the axis ratio,  $c/a$ . To check if the observed trend with lookback time is due to this effect, we calculate the time evolution of the ratio between the minor and major axes of the reduced moment of inertia tensor of the system. This is obtained by modifying Eq. (1) to include a weight,  $w_i = 1/d_i^2$ , for each satellite, where  $d_i$  is the distance of the satellite from the central galaxy. This ensures that all satellites contribute equally to the reduced moment of inertia of the system. The evolution of the reduced  $\langle c/a \rangle$  axes ratio is shown in the bottom-left-hand panel of Fig. 7. We find the same qualitative trend, that the median axes ratio decreases towards the past, with a minimum  $\sim 10$  Gyrs ago. Thus, the minimum seen in the left-hand column of Fig. 7 is physical and indicates a pronounced flattening of the progenitor system at redshift,  $z \sim 1.5$ .

The lookback time corresponding to the minimum of  $\langle c/a \rangle$

coincides with the typical accretion time of these satellites; half of the present-day satellites were accreted more than 8.5 Gyrs ago (Shao et al. 2018a). This paints an intriguing picture for the evolution of the satellite progenitors: starting at high redshift,  $z > 3$ , they first move towards the cosmic web sheet that surrounds the progenitor of their  $z = 0$  host, and, once there, they move in the plane of this sheet towards their present-day host. This is a manifestation of the anisotropic gravitational collapse of matter, with overdensities first collapsing along one dimension to form large-scale sheets, then along a second dimension to form filaments, and finally collapsing along the last direction to produce virialized haloes (Zel'dovich 1970; Arnold et al. 1982; Icke 1973). Once inside the host, the satellite system becomes thicker with time. This thickening could be due to the satellites moving on different orbital planes already at the time of accretion, as well as to torques and interactions inside the host halo that can modify the orbital plane of satellites, as we have seen in Figs. 5 and 6.

The picture of anisotropic gravitational collapse raises an interesting question: once the satellite progenitors are distributed in a plane, do they further evolve into a filamentary configurations before falling into their host halo? We investigate this in the top-right-hand panel of Fig. 7, which shows the time evolution of the median

axes ratio,  $\langle b/a \rangle$ . This is a measure of how filamentary a distribution is, with small  $b/a$  values corresponding to thin filaments. The plot shows that on average the  $b/a$  ratio was smaller in the past, reaching at minimum  $\sim 7$  Gyrs ago. To interpret this result, we also need to study the evolution of the same axis ratio but for the reduced moment of inertia, which is shown in the bottom-right-hand panel of Fig. 7. Interestingly, the  $\langle b/a \rangle$  ratio for the reduced moment of inertia shows only a minor decrease at high redshift. This indicates that the distribution of satellite progenitors does not show strong evolution of its filamentary character, that is not all satellites are accreted along the same filament. This is in agreement with previous studies which have shown that most MW-mass haloes accrete their brightest satellites from three or more different filaments (e.g. Libeskind et al. 2005; González & Padilla 2016; Shao et al. 2018a). Note that, according to the left-hand column of Fig. 7, these multiple filaments are preferentially found in the same plane (see also Danovich et al. 2012; Libeskind et al. 2014; Shao et al. 2018a).

#### 4.2.2 The flattening of systems with planes of satellites

We now investigate the time evolution of the  $c/a$  and  $b/a$  axes ratios for systems that at the present day host a *MW-like-thin* or *MW-like-orbit* plane of satellites. These are shown in Fig. 7 as dotted and solid lines, respectively.

By selection, *MW-like-thin* systems are very thin at  $z = 0$ ; however, their median  $c/a$  axes ratio grows rapidly with lookback time. This indicates that most of these systems are chance alignments of satellites that do not preserve a low  $c/a$  value for an extended period of time (see also Bahl & Baumgardt 2014; Gillet et al. 2015; Buck et al. 2016). After the initial increase, the  $\langle c/a \rangle$  of *MW-like-thin* systems traces very well the time variation of  $\langle c/a \rangle$  for the overall MW-mass population, although the exact value is systematically lower by  $\sim 0.05$ . This indicates that *MW-like-thin* satellite systems were on average more planar than the overall population of satellites of MW-mass haloes at all redshifts. The *MW-like-thin* sample shows a similar time evolution in the  $\langle b/a \rangle$  ratio, which, except for the last 1 Gyr, traces very well the  $\langle b/a \rangle$  value of the full population, albeit at a systematically lower value.

*MW-like-orbit* systems have, at  $z = 0$ , a larger  $\langle c/a \rangle$  value than the *MW-like-thin* sample; however, since the latter increases rapidly, it catches up and both have roughly equal  $c/a$  values between 1 and 6 Gyrs ago. Even further in the past, the *MW-like-orbit* systems are systematically thinner than the *MW-like-thin* ones. The two samples have only 30% of their members in common and thus the close match between the two  $c/a$  ratios is unexpected. Even more surprising is that the  $b/a$  axes ratios of the two samples are roughly equal for lookback times above 1 Gyr.

We also studied the evolution of  $\langle c/a \rangle$  and  $\langle b/a \rangle$  for the small sample of systems that fulfil both the *MW-like-thin* and *MW-like-orbit* selection criteria. For clarity, we do not show these results in Fig. 7. The combined systems have the same axes ratio as the *MW-like-thin* sample for lookback times less than 1 Gyr, after which their time evolution matches very closely that of the *MW-like-orbit* sample, albeit with some scatter due to the small sample size.

#### 4.2.3 The flattening of satellite systems at infall

Present day planes of satellites correspond to satellite systems that were systematically thinner at  $z > 0$  and especially at the time when most satellites were accreted. This raises an intriguing question: do planes of satellites form in the host haloes where satellite infall was most anisotropic? Such a picture has been suggested

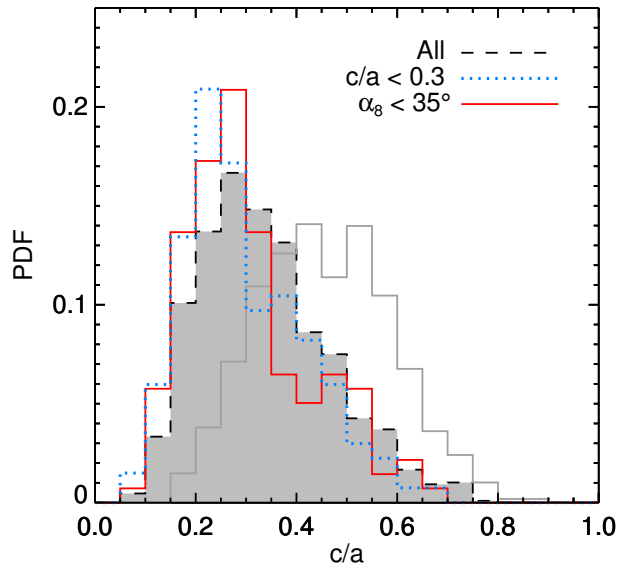


**Figure 8.** The distribution of axes ratios,  $c/a$ , for satellite entry points into their  $z = 0$  MW-mass hosts. The entry points are calculated at the time of accretion into the FOF halo of the MW-mass host progenitor. The light grey curve shows the distribution of the satellite system  $c/a$  at  $z = 0$ .

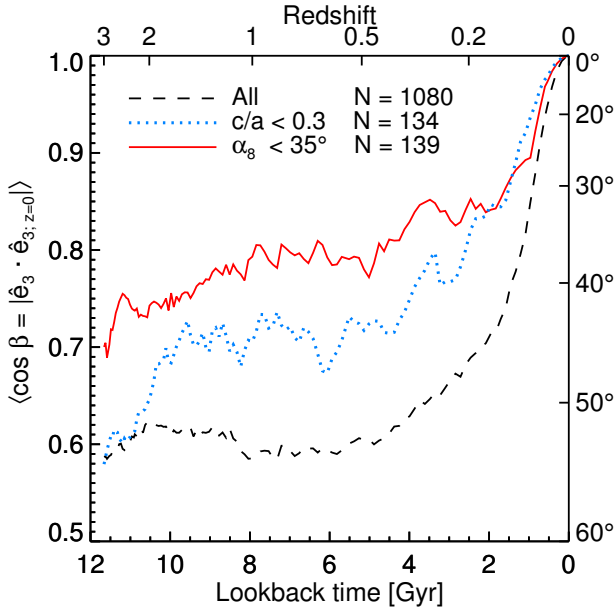
by previous studies (e.g. Libeskind et al. 2005; Buck et al. 2015). However, since they employed very small samples of haloes, such studies lacked the statistical power to give a definitive answer. We investigate this question in Fig. 8, which shows the distribution of  $c/a$  axes ratios for the satellites' entry points into their host. A satellite's entry point is defined as the position of its progenitor at the time it first entered the progenitor FOF halo of its MW-mass host. The entry position is calculated with respect to the host halo centre at infall time. The distribution of  $c/a$  at infall cannot be directly compared to the results in Fig. 7 since the classical satellites of MW-mass hosts have a wide range of infall times (see Fig. 12 in Shao et al. 2018a).

Fig. 8 shows that the galactic satellites formed a more flattened distribution at infall than at the present time (compare the dashed with the grey solid lines), and supports our conclusion that the orbital evolution of satellites typically leads to more isotropic distributions at  $z = 0$  (see also Bowden et al. 2013). In particular, the small  $c/a$  values at infall reflect the anisotropic nature of the large-scale mass distribution surrounding a MW-mass halo (see e.g. Lovell et al. 2011; Cautun et al. 2014; Libeskind et al. 2014; Shao et al. 2016).

The two subsamples with present-day MW-like satellite distributions had even lower values  $c/a$  at infall than the overall population, but the difference is rather small. In particular, some *MW-like-thin* and *MW-like-orbit* systems had infall  $c/a$  ratios of 0.5 or higher, while many satellite systems with  $c/a \sim 0.2$  at infall did not evolve into present day MW-like satellite populations. This suggests that highly anisotropic accretion is just one of a number of processes that lead to the formation of planes of satellite galaxies, and that it might not even be the dominant factor.

#### 4.2.4 The directional coherence of satellite systems

We now study how the orientation of the satellite systems changes with time. For this, we consider the eigenvector,  $\hat{e}_3$ , that points along the minor axis of the satellite distribution. Fig. 9 shows the



**Figure 9.** The directional coherence of the minor axis,  $\hat{e}_3$ , of the satellite distribution. It shows the time evolution of the median misalignment angle,  $\beta$ , between  $\hat{e}_3$  at different lookback times and its present-day value,  $\hat{e}_{3,z=0}$ . The three lines correspond to the overall population of MW-mass haloes as well as to  $z = 0$  systems that have *MW-like-thin* and *MW-like-orbit* planes of satellites. A complete lack of alignment corresponds to  $\langle \cos \beta \rangle = 0.5$ .

evolution of the median misalignment angle,  $\beta$ , between  $\hat{e}_3$  at different epochs and its value at  $z = 0$ . For the full sample,  $\beta$  increases rapidly with lookback time, reaching a value of  $\langle \beta \rangle \sim 45^\circ$  at 2 Gyrs, and then tends to a constant value,  $\langle \beta \rangle \sim 55^\circ$ , further in the past. The value of  $\langle \beta \rangle$  is slightly lower than in the case of no alignment, for which  $\langle \beta \rangle = 60^\circ$ , and indicates a weak directional coherence between the shape of the present-day satellite system and that of its progenitors. Thus, in general, both the axes ratio,  $c/a$ , and the minor axis orientation,  $\hat{e}_3$ , show a large and rapid variation with time.

The shape of *MW-like-thin* satellite systems shows more directional coherence across time than the full population, with the median misalignment angle at large lookback times tending to a constant value,  $\langle \beta \rangle \sim 45^\circ$ . The stronger alignment is due to *MW-like-thin* systems having a higher fraction of satellites that share the same orbital plane (see e.g. Fig. 4) that helps to preserve the directional coherence of the distribution. This hypothesis is supported by the time dependence of  $\langle \beta \rangle$  for the *MW-like-orbit* subsample, which shows even better coherence across time than the *MW-like-thin* systems. After an initial rapid increase in the misalignment angle, the *MW-like-orbit* systems have  $\langle \beta \rangle \sim 35^\circ$  that grows slowly with lookback time.

### 4.3 Evolution of the satellites with co-planar orbits

We now investigate the driving factors that lead to many satellites having nearly co-planar orbits. In particular, we focus on *MW-like-orbit* systems, for which at least 8 of the 11 brightest satellites orbit within a narrow plane. In Section 4.1.2 we studied two examples of such planes: in the first one, the 8 co-planar satellites had been orbiting in the same plane for the last 8 Gyrs, while in the second example the co-planar configuration was formed only recently. In

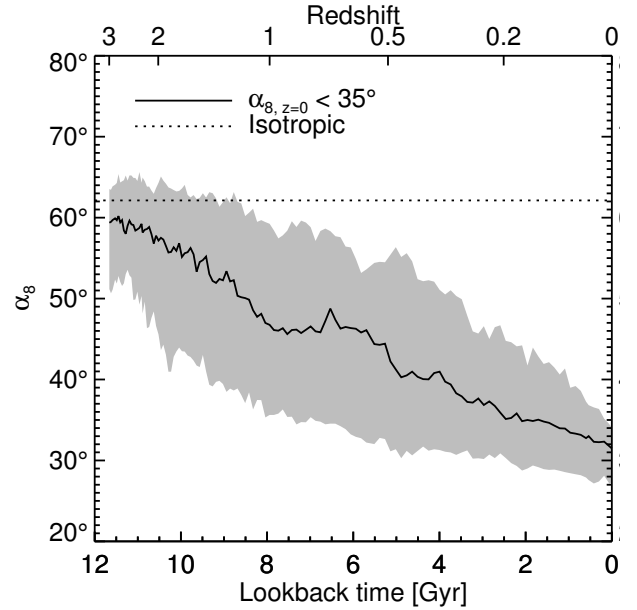


**Figure 10.** The time evolution of the opening angle,  $\alpha_8$ , that encloses the orbital poles of 8 of the top 11 satellites with the most co-planar orbits at the present day. We show results only for the subsample with  $\alpha_8 \leq 35^\circ$  at  $z = 0$ . The solid line shows the median value of  $\alpha_8$  while the shaded region shows the 16 to 84 percentiles of the distribution. The horizontal dotted line marks the mean angle for an isotropic distribution of orbits.

Fig. 10 we study which of the two examples describes the typical formation history of a *MW-like-orbit* system. Here we plot, as a function of time, the smallest opening angle,  $\alpha_8$ , needed to enclose the orbital poles of the 8 satellites with the most co-planar orbits at the present day.

Fig. 10 shows that the median value of  $\alpha_8$  increases with lookback time, from  $31.5^\circ$  at  $z = 0$  to  $\sim 50^\circ$  at  $z = 1$ . By construction, the median value of  $\alpha_8$  at the present day is low because we are considering only *MW-like-orbit* systems which have  $\alpha_8 \leq 35^\circ$  today. We conclude that, on average, configurations of 8 satellites with co-planar orbits today must have formed recently. In particular, if we take the formation time as the point when  $\alpha_8$  falls below  $40^\circ$ , we find that half of the systems formed less than 4 Gyrs ago. However, there is large variability amongst individual systems, as indicated by the grey shaded region in Fig. 10, which shows the 16 and 84 percentiles of the distribution. At one extreme, the 16 percentile line remains below  $\alpha_8 = 40^\circ$  for the past 9 Gyrs, while, at the other extreme, the 84 percentile line is below  $\alpha_8 = 40^\circ$  only for the past 1 Gyr. Thus, there is an important population of both very old and very young *MW-like-orbit* planes of satellites. We note that individual systems show short term variations in  $\alpha_8$  on top of the long-term trend of decreasing  $\alpha_8$  with time; this makes it difficult to determine unambiguously the formation time of a given plane.

The time variation of the average  $\alpha_8$  opening angle is roughly constant (notwithstanding some variability on very short timescales). This suggests that the dominant processes which lead to co-planar satellite orbits are acting consistently over long periods of time. In Section 4.1.1 we saw that massive satellites can induce radical changes in the orbital planes of other satellites. However, while such changes might nudge a satellite orbit to the common orbital plane of other dwarfs, on average massive satellites increase the dispersion of orbital poles and thus contribute to destroying co-planar satellite distributions (e.g. see Fernando et al. 2018). More-

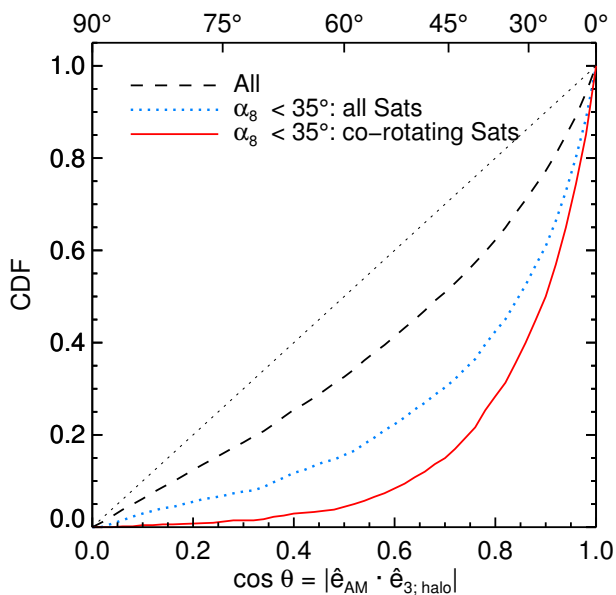


**Figure 11.** The alignment of the satellite orbital poles with the minor axis of their host halo. The graph shows the CDF of the cosine of the misalignment angle,  $\cos \theta$ , between the  $z = 0$  orbital angular momentum of satellites and the minor axis of their host halo. The dashed line shows the distribution for the brightest 11 satellites around all MW-mass hosts. The other two curves show results for *MW-like-orbit* systems (i.e. systems with  $\alpha_8 < 35^\circ$ ); the dotted line is for all 11 satellites of these systems, while the solid line is for the 8 satellites with the most co-planar orbits.

over, satellite–satellite interactions are one of the main factors that determine short-term variability in  $\alpha_8$  for individual systems.

#### 4.3.1 The host halo as a driver of co-planar satellite orbits

The host haloes of galactic satellites are triaxial and this gives rise to torques that act upon the satellites. The effect of these torques is complex and depends on the orientation of a satellite’s orbital pole with respect to its host halo (see e.g. Bowden et al. 2013; Erkal et al. 2016; Fernando et al. 2017). Orbital planes are approximately stable in a triaxial halo only if they lie within the equatorial or polar planes of the host halo. For all other orientations, the orbit of a satellite can be thought of in terms of box orbits and shows complex time variability (see e.g. Pontzen et al. 2015). These considerations suggest that the properties of the host halo could play an important role in the formation and survival of co-planar satellite distributions.

We investigate the role of the host halo in Fig. 11. This shows the cumulative distribution function (CDF) of the alignment angle between the orbital poles of satellites and the minor axis of their host halo. We can see that the overall population of satellites shows mild alignment with the host halo, with a preference for satellites to rotate within the equatorial plane of their host (Lovell et al. 2011; Cautun et al. 2015a). The strength of the alignment can be gauged by comparing with the dotted light grey line, which shows the case of no alignment. The alignment between satellite orbital poles and host halo is a manifestation of anisotropic accretion as well as the torquing of orbits by the aspherical mass distribution of the host.

Interestingly, the satellites of *MW-like-orbit* systems show a much stronger alignment with their host haloes than the overall satellites populations. To some extent, this would have been

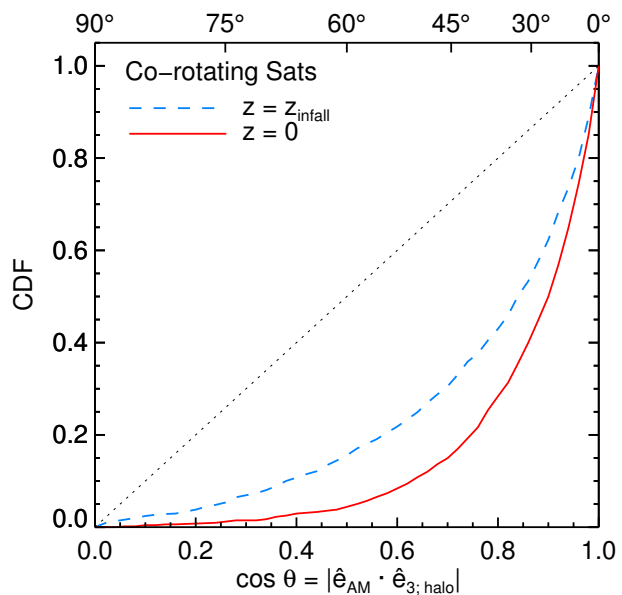


**Figure 12.** The alignment of the satellites with co-planar orbits and the minor axis of their host halo. The graph shows the alignment of the angular momentum of the satellites at infall (dashed line) and of their present-day angular momentum (solid line). The stronger alignment for the  $z = 0$  orbital poles of co-planar satellites indicates that torques induced by the host halo are critical for the formation of rotating planes of satellites.

expected since satellites in *MW-like-orbit* systems experience a greater degree of anisotropic accretion (see Fig. 8). However, the difference in the alignment strength seems larger than the difference in the distribution of  $c/a$  values at infall (see Fig. 8), suggesting that additional physical processes are at play. If we further restrict our analysis to the satellites of *MW-like-orbit* systems that share the same orbital planes (solid line in Fig. 11), we find an even stronger alignment between the orbital poles and the host’s minor axis. This suggests that co-planar satellites orbit preferentially in the equatorial plane of their host halo. We study this topic in more detail in a companion paper, Shao et al. (2019), where we show that in the vast majority of cases, the normal to the plane in which the 8 co-planar satellite rotate is within  $30^\circ$  of the halo minor axis.

We now investigate if torques arising from the aspherical mass distribution of the host halo contribute to the formation and stability of co-rotating planes of satellites. On average, the torques tend to move satellite orbits towards the host’s equatorial plane and thus this process would leave the following two signatures: i) co-rotating planes should lie close to the host halo’s equatorial plane, and ii) after infall, the orbital plane of each co-planar satellite should be systematically tilted towards the host’s equatorial plane. Fig. 11 shows that co-planar satellites are well aligned with the host’s minor axis and thus provides evidence for the first signature of torques. However, a similar alignment could result from the anisotropic accretion of satellites, if the satellites entry points were found preferentially along the host’s equatorial plane (Libeskind et al. 2014; Shao et al. 2018a). To prove beyond doubt the role of the host halo, we need to check the second signature, which we do in Fig. 12.

Fig. 12 shows the change in a satellite’s orbital pole between infall and the present day, which we measure with respect to the present-day host’s minor axis. For clarity, we restrict the analysis to the 8 co-planar satellites of *MW-like-orbit* systems. The figure shows that the orbital poles of satellites are better aligned with their

host halo at the present than at infall, thus supporting the hypothesis that tides resulting from the triaxial shape of the host halo are important for the formation of rotating planes of satellite galaxies. While not shown, we have performed other tests that support the same conclusion. For example, the alignment between the orbital poles of satellites with co-planar orbits and the minor axis of their host halo always increases with time. Furthermore, the fraction of *MW-like-orbit* systems increases with time from 7.3% at  $z = 2$  to 11.3% at the present day, which indicates that late-time processes play an essential role in enhancing the number of satellites with co-planar orbits.

## 5 CONCLUSIONS

We have used the EAGLE hydrocosmological simulation to study the formation and evolution of planes of satellite galaxies similar to the plane observed in the Milky Way. We have analysed the MW classical dwarfs since these represent an observationally complete sample of satellites that, moreover, are massive enough to be well resolved in the EAGLE simulation. Our sample consists of 1080 systems with a typical halo mass of  $\sim 10^{12} M_{\odot}$  that have at least 11 luminous satellites within a distance of 300 kpc from the centre.

To better understand the MW's satellite distribution, we have focused on its two defining characteristics: its thinness and its high degree of co-planar satellite orbits. To study thin planes of satellites we have defined the *MW-like-thin* subsample which consists of EAGLE satellite systems with minor-to-major axes ratios,  $c/a \leq 0.3$ . To characterise co-planar orbits, we have devised a new, robust formalism that identifies the subsets of satellites with the most co-planar orbits. Out of the 11 MW classical satellites, 8 have highly clustered orbital poles that are contained within a  $21.9^{\circ}$  opening angle centred around  $(l, b) = (182.3^{\circ}, -1.8^{\circ})$ . The other 3 satellites – Sextans, Leo I and Sagittarius – have orbital poles roughly perpendicular to this direction. The 8 Galactic satellites with co-planar orbits stand out when compared to both isotropic and to average  $\Lambda$ CDM satellite distributions. To study these systems, we defined a *MW-like-orbit* subsample as those systems for which at least 8 out of the brightest 11 satellites have orbital poles contained within a  $35^{\circ}$  opening angle. In order to obtain large enough samples we deliberately adopt criteria for identifying *MW-like* planes that are less extreme than the corresponding properties of the MW. Both our *MW-like-thin* and *MW-like-orbit* subsamples were selected to contain  $\sim 100$  or more systems and thus they allow us to infer statistically robust results. We expect that similar processes to those that operate on our less extreme systems will have also operated in the real MW.

Our main conclusions may be summarised as follows:

- (i) Most satellites have slowly-varying orbital planes; however there is a substantial population that experiences rapid and drastic changes in orbits. Most such events are due to close encounters with other massive satellites (see centre panels in Fig. 5 and 6).
- (ii) On average, satellite systems were flatter in the past, with a minimum  $c/a$  axis ratio around 9 Gyrs ago (see Fig. 7). This lookback time corresponds to the typical infall time of the classical satellites and suggests that the progenitors of the present-day satellites first collapsed onto a large-scale sheet before falling into their host haloes. After infall, satellite systems are characterised by increasingly higher  $c/a$  ratios (see Fig. 8).
- (iii) *MW-like-thin* planes of satellites are short-lived chance associations whose thickness increases on a timescale of less than

1 Gyr. However, such systems are at all times flatter than the overall satellite system population (see Fig. 7).

(iv) Both *MW-like-thin* and *MW-like-orbit* systems were, on average, flatter at infall than the overall population of galactic satellites (see Fig. 8). However, a highly anisotropic satellite infall does not guarantee the formation of a plane of satellites, indicating that anisotropic accretion is just one of the processes that result in the formation of planes of satellites.

(v) We find a poor correlation between the direction of planes of satellites at two different epochs. The correlation is stronger for *MW-like-orbit* systems where many satellites rotate in the same plane, but even in this case, the misalignment angle is  $\geq 35^{\circ}$  after just 2 Gyrs (see Fig. 9).

(vi) Satellites that orbit within the same plane have not always done so and around half of them formed a plane within the last  $\sim 4$  Gyrs. There is a large system-to-system variation, with significant fractions forming both recently and as long as 9 Gyrs ago (see Fig. 10).

(vii) Co-planar satellites orbit preferentially within the equatorial plane of their host halo (see Fig. 11). The torques resulting from the aspherical mass distribution of the hosts play an important role in the formation of rotating planes of satellites (see Fig. 12).

One of the goals of this paper has been to understand the Galactic plane of classical satellites. Our results indicate that the flattening of the MW satellite distribution is short lived (see also Lipnicky & Chakrabarti 2017) and likely due to a chance occurrence. In contrast, the large number of satellites, 8 out of the 11 classical dwarfs, that share the same orbital plane is physically more interesting. We predict that a majority of these 8 satellites have been orbiting within the same plane for many billions of years. In particular, the EAGLE simulation predicts that a smaller opening angle enclosing the orbital poles of the 8 co-planar satellites corresponds to an older rotating plane of satellites. The MW opening angle lies in the tail of the distribution and thus indicates a very long-lived rotating plane composed of 8 out of the 11 classical satellites. Note, however, that at least two of its members, the LMC and the SMC, are thought to be recent additions to the MW satellite system (Besla et al. 2007; Kallivayalil et al. 2013; Patel et al. 2017). For these two galaxies, we predict that their orbital angular momentum has pointed roughly in the same direction since long before their infall into the MW.

From a practical perspective, the 8 satellites with co-planar orbits can be used to infer, with high precision, the orientation of the Galactic dark matter halo, as we show in a companion paper (Shao et al. 2019). Furthermore, the halo tidal field plays an important role in the formation of co-planar satellites and better understanding this process could lead to additional inferences about the Galactic dark matter halo and its relation to the cosmic web around our galaxy.

While we infer an early formation time for the Galactic subset of the 8 satellites with co-planar orbits, its future could be short-lived. This is a consequence of the recent accretion of the LMC, whose massive dark matter halo (Peñarrubia et al. 2016; Shao et al. 2018b) can induce dramatic changes in the orbital planes of the other dwarfs. This is especially true if close encounters occur; observational data already shows that this likely happened recently for the Tucana III stream (Erkal et al. 2018). Luckily, the LMC is predicted to merge with our galaxy in the next  $\sim 2.5$  Gyrs (Cautun et al. 2019); this may allow the subset of co-planar satellites to survive unscathed, albeit with at least one fewer member.

## ACKNOWLEDGEMENTS

We thank the anonymous referee for detailed comments that have helped us improve the paper. SS, MC and CSF were supported by the Science and Technology Facilities Council (STFC) [grant number ST/I00162X/1, ST/P000541/1] and by the ERC Advanced Investigator grant, DMIDAS [GA 786910]. SS is also supported by the ERC grant ERC-StG-716532-PUNCA. This work used the DiRAC@Durham facility managed by the Institute for Computational Cosmology on behalf of the STFC DiRAC HPC Facility ([www.dirac.ac.uk](http://www.dirac.ac.uk)). The equipment was funded by BEIS capital funding via STFC capital grants ST/K00042X/1, ST/P002293/1, ST/R002371/1 and ST/S002502/1, Durham University and STFC operations grant ST/R000832/1. DiRAC is part of the National e-Infrastructure.

## REFERENCES

- Agustsson I., Brainerd T. G., 2010, *ApJ*, **709**, 1321
- Ahmed S. H., Brooks A. M., Christensen C. R., 2017, *MNRAS*, **466**, 3119
- Arnold V. I., Shandarin S. F., Zeldovich I. B., 1982, *Geophysical and Astrophysical Fluid Dynamics*, **20**, 111
- Aubert D., Pichon C., Colombi S., 2004, *MNRAS*, **352**, 376
- Bahl H., Baumgardt H., 2014, *MNRAS*, **438**, 2916
- Banik I., O’Ryan D., Zhao H., 2018, *MNRAS*, **477**, 4768
- Besla G., Kallivayalil N., Hernquist L., Robertson B., Cox T. J., van der Marel R. P., Alcock C., 2007, *ApJ*, **668**, 949
- Bowden A., Evans N. W., Belokurov V., 2013, *MNRAS*, **435**, 928
- Brainerd T. G., 2005, *ApJ*, **628**, L101
- Buck T., Macciò A. V., Dutton A. A., 2015, *ApJ*, **809**, 49
- Buck T., Dutton A. A., Macciò A. V., 2016, *MNRAS*, **460**, 4348
- Callingham T. M., et al., 2019, *MNRAS*, **484**, 5453
- Cautun M., Frenk C. S., 2017, *MNRAS*, **468**, L41
- Cautun M., van de Weygaert R., Jones B. J. T., Frenk C. S., 2014, *MNRAS*, **441**, 2923
- Cautun M., Wang W., Frenk C. S., Sawala T., 2015a, *MNRAS*, **449**, 2576
- Cautun M., Bose S., Frenk C. S., Guo Q., Han J., Hellwing W. A., Sawala T., Wang W., 2015b, *MNRAS*, **452**, 3838
- Cautun M., Deason A. J., Frenk C. S., McAlpine S., 2019, *MNRAS*, **483**, 2185
- Conn A. R., et al., 2013, *ApJ*, **766**, 120
- Crain R. A., et al., 2015, *MNRAS*, **450**, 1937
- Danovich M., Dekel A., Hahn O., Teyssier R., 2012, *MNRAS*, **422**, 1732
- Davis M., Efstathiou G., Frenk C. S., White S. D. M., 1985, *ApJ*, **292**, 371
- Deason A. J., et al., 2011, *MNRAS*, **415**, 2607
- Dolag K., Borgani S., Murante G., Springel V., 2009, *MNRAS*, **399**, 497
- Erkal D., Sanders J. L., Belokurov V., 2016, *MNRAS*, **461**, 1590
- Erkal D., et al., 2018, *MNRAS*, **481**, 3148
- Fernando N., Arias V., Guglielmo M., Lewis G. F., Ibata R. A., Power C., 2017, *MNRAS*, **465**, 641
- Fernando N., Arias V., Lewis G. F., Ibata R. A., Power C., 2018, *MNRAS*, **473**, 2212
- Fritz T. K., Battaglia G., Pawlowski M. S., Kallivayalil N., van der Marel R., Sohn S. T., Brook C., Besla G., 2018, *A&A*, **619**, A103
- Gaia Collaboration et al., 2018, *A&A*, **616**, A12
- Gillet N., Ocvirk P., Aubert D., Knebe A., Libeskind N., Yepes G., Gottlöber S., Hoffman Y., 2015, *ApJ*, **800**, 34
- Gómez F. A., Besla G., Carpintero D. D., Villalobos Á., O’Shea B. W., Bell E. F., 2015, *ApJ*, **802**, 128
- González R. E., Padilla N. D., 2016, *ApJ*, **829**, 58
- Hammer F., Yang Y., Fouquet S., Pawlowski M. S., Kroupa P., Puech M., Flores H., Wang J., 2013, *MNRAS*, **431**, 3543
- Hodkinson B., Scholtz J., 2019, arXiv e-prints,
- Ibata R. A., et al., 2013, *Nature*, **493**, 62
- Icke V., 1973, *A&A*, **27**, 1
- Jiang L., Helly J. C., Cole S., Frenk C. S., 2014, *MNRAS*, **440**, 2115
- Kallivayalil N., van der Marel R. P., Besla G., Anderson J., Alcock C., 2013, *ApJ*, **764**, 161
- Kang X., Mao S., Gao L., Jing Y. P., 2005, *A&A*, **437**, 383
- Knebe A., Gill S. P. D., Gibson B. K., Lewis G. F., Ibata R. A., Dopita M. A., 2004, *ApJ*, **603**, 7
- Kroupa P., Theis C., Boily C. M., 2005, *A&A*, **431**, 517
- Kunkel W. E., Demers S., 1976, in Dickens R. J., Perry J. E., Smith F. G., King I. R., eds, *Royal Greenwich Observatory Bulletins Vol. 182, The Galaxy and the Local Group*. p. 241
- Li Y.-S., Helmi A., 2008, *MNRAS*, **385**, 1365
- Libeskind N. I., Frenk C. S., Cole S., Helly J. C., Jenkins A., Navarro J. F., Power C., 2005, *MNRAS*, **363**, 146
- Libeskind N. I., Cole S., Frenk C. S., Okamoto T., Jenkins A., 2007, *MNRAS*, **374**, 16
- Libeskind N. I., Frenk C. S., Cole S., Jenkins A., Helly J. C., 2009, *MNRAS*, **399**, 550
- Libeskind N. I., Knebe A., Hoffman Y., Gottlöber S., 2014, *MNRAS*, **443**, 1274
- Lipnicky A., Chakrabarti S., 2017, *MNRAS*, **468**, 1671
- Lovell M. R., Eke V. R., Frenk C. S., Jenkins A., 2011, *MNRAS*, **413**, 3013
- Lynden-Bell D., 1976, *MNRAS*, **174**, 695
- Lynden-Bell D., 1982, *The Observatory*, **102**, 202
- McAlpine S., et al., 2016, *Astronomy and Computing*, **15**, 72
- McConnachie A. W., 2012, *AJ*, **144**, 4
- Metz M., Kroupa P., Libeskind N. I., 2008, *ApJ*, **680**, 287
- Metz M., Kroupa P., Theis C., Hensler G., Jerjen H., 2009, *ApJ*, **697**, 269
- Müller O., Pawlowski M. S., Jerjen H., Lelli F., 2018, *Science*, **359**, 534
- Newton O., Cautun M., Jenkins A., Frenk C. S., Helly J. C., 2018, *MNRAS*, **479**, 2853
- Nierenberg A. M., Auger M. W., Treu T., Marshall P. J., Fassnacht C. D., Busha M. T., 2012, *ApJ*, **752**, 99
- Patel E., Besla G., Sohn S. T., 2017, *MNRAS*, **464**, 3825
- Pawlowski M. S., 2016, *MNRAS*, **456**, 448
- Pawlowski M. S., Kroupa P., 2013, *MNRAS*, **435**, 2116
- Pawlowski M. S., Kroupa P., Angus G., de Boer K. S., Famaey B., Hensler G., 2012, *MNRAS*, **424**, 80
- Pawlowski M. S., et al., 2014, *MNRAS*, **442**, 2362
- Pawlowski M. S., et al., 2017, *Astronomische Nachrichten*, **338**, 854
- Peñarrubia J., Gómez F. A., Besla G., Erkal D., Ma Y.-Z., 2016, *MNRAS*, **456**, L54
- Piatek S., Pryor C., Olszewski E. W., 2016, *AJ*, **152**, 166
- Planck Collaboration XVI 2014, *A&A*, **571**, A16
- Pontzen A., Read J. I., Teyssier R., Governato F., Gualandris A., Roth N., Devriendt J., 2015, *MNRAS*, **451**, 1366
- Schaye J., et al., 2015, *MNRAS*, **446**, 521
- Shao S., Cautun M., Frenk C. S., Gao L., Crain R. A., Schaller M., Schaye J., Theuns T., 2016, *MNRAS*, **460**, 3772
- Shao S., Cautun M., Frenk C. S., Grand R. J. J., Gómez F. A., Marinacci F., Simpson C. M., 2018a, *MNRAS*, **476**, 1796
- Shao S., Cautun M., Deason A. J., Frenk C. S., Theuns T., 2018b, *MNRAS*, **479**, 284
- Shao S., Cautun M., Deason A. J., Frenk C. S., 2019, in prep.
- Shaya E. J., Tully R. B., 2013, *MNRAS*, **436**, 2096
- Shi J., Wang H., Mo H. J., 2015, *ApJ*, **807**, 37
- Smith R., Duc P. A., Bournaud F., Yi S. K., 2016, *ApJ*, **818**, 11
- Sohn S. T., Besla G., van der Marel R. P., Boylan-Kolchin M., Majewski S. R., Bullock J. S., 2013, *ApJ*, **768**, 139
- Springel V., Yoshida N., White S. D. M., 2001, *New Astron*, **6**, 79
- Tully R. B., Libeskind N. I., Karachentsev I. D., Karachentseva V. E., Rizzi L., Shaya E. J., 2015, *ApJ*, **802**, L25
- Wang J., Frenk C. S., Cooper A. P., 2013, *MNRAS*, **429**, 1502
- Wang Y. O., Lin W. P., Kang X., Dutton A., Yu Y., Macciò A. V., 2014, *ApJ*, **786**, 8
- Yang X., van den Bosch F. C., Mo H. J., Mao S., Kang X., Weinmann S. M., Guo Y., Jing Y. P., 2006, *MNRAS*, **369**, 1293
- Zel’dovich Y. B., 1970, *A&A*, **5**, 84
- Zentner A. R., Kravtsov A. V., Gnedin O. Y., Klypin A. A., 2005, *ApJ*, **629**, 219